

Cite this: *Lab Chip*, 2012, 12, 2337–2344

www.rsc.org/loc

PAPER

Measuring acoustic energy density in microchannel acoustophoresis using a simple and rapid light-intensity method†

Rune Barnkob,^{*a} Ida Iranmanesh,^b Martin Wiklund^b and Henrik Bruus^a

Received 3rd February 2012, Accepted 13th March 2012

DOI: 10.1039/c2lc40120g

We present a simple and rapid method for measuring the acoustic energy density in microchannel acoustophoresis based on light-intensity measurements of a suspension of particles. The method relies on the assumption that each particle in the suspension undergoes single-particle acoustophoresis. It is validated by the single-particle tracking method, and we show by proper re-scaling that the re-scaled light intensity plotted *versus* re-scaled time falls on a universal curve. The method allows for analysis of moderate-resolution images in the concentration range encountered in typical experiments, and it is an attractive alternative to particle tracking and particle image velocimetry for quantifying acoustophoretic performance in microchannels.

I. Introduction

Acoustofluidics and ultrasound handling of particle suspensions is a research field in rapid growth both concerning physical characterization and optimization of the devices as well as biological applications.^{1,2} When designing a microchip for microchannel acoustophoresis, the acoustic energy density inside the microchannel is an important parameter. For example, the energy density scales the acoustic radiation forces acting on suspended particles or cells and can therefore be used as a figure of merit of the acoustophoretic performance. However, it is neither straightforward to theoretically predict, nor experimentally determine the energy density in the microchannel. The acoustic power sent from the transducer to the microchannel is subject to losses from thermal dissipation and acoustic radiation, making it difficult to predict the acoustic energies inside the microchannel from a given input power of the actuating transducer. Moreover, it is difficult to model the exact actuated acoustic resonance and therefore difficult to predict the distribution of energy between the microchannel and the surrounding microchip.

Existing techniques for measuring the acoustic energy density (or acoustic pressure amplitude) mostly rely on external electric³ or gravitational^{4,5} forces. However, based on the acoustophoretic alignment of particles advected along a microchannel, Wiklund *et al.*⁶ estimated the acoustic pressure amplitude using the advection length and advection time needed to align the particles, and Barnkob *et al.*⁷ measured the acoustic energy

density relying solely on the acoustophoretic motion of the particles. The latter method based on single-particle tracking is particularly suited for low particle concentrations and provides an important step in measuring compressibilities of individual cells using acoustophoresis.^{8–10} Later, Augustsson *et al.*¹¹ used acoustophoretic velocity fields measured by micro-particle-image velocimetry (micro-PIV) to determine the energy density as function of position across an entire microscope field of view with a relative uncertainty of less than 2%. Although these methods each have their individual strengths, there exists none for simple and rapid determination of the acoustic energy density.

In this work we present a simple, rapid and inexpensive light-intensity-based method for measuring the acoustic energy density E_{ac} in microchannel acoustophoresis with the primary motive to characterize the performance of an acoustophoresis microchip. The measured light intensity originates from transillumination light microscopy operated at moderate resolution. The theoretical foundation and an experimental realization of the method are described, and the method is validated by comparing the measured E_{ac} with that obtained by the single-particle tracking method.⁷ Furthermore, the new method yields the expected scaling of E_{ac} with the applied piezo transducer voltage to the power 2. Also, it is shown theoretically that by proper re-scaling, the re-scaled intensity plotted *versus* re-scaled time should fall on a universal curve. This universality is successfully tested experimentally. We end by discussing the limitations of the method.

II. Single-particle theory

We study a glass–silicon–glass chip containing an optically transparent microchannel filled with a particle suspension, as described in more detail in Section V. The channel is illuminated from the top, and the transmitted light is recorded by a CCD

^aDepartment of Micro- and Nanotechnology, Technical University of Denmark DTU Nanotech Building 345 East, DK-2800, Kongens Lyngby, Denmark. E-mail: barnkob@alumni.dtu.dk

^bDepartment of Applied Physics, Royal Institute of Technology, AlbaNova University Center, SE-106 91, Stockholm, Sweden

† Electronic supplementary information (ESI) available. See DOI: 10.1039/c2lc40120g/

camera mounted on a mid-range microscope using a low-numerical-aperture objective (N.A. = 0.25, focal depth $\approx 10 \mu\text{m}$). The particles appear as blurred black/gray spots covering about 10 pixels on the resulting images. The microchip is ultrasonically actuated by attaching a piezo transducer to the chip and driving it with a voltage U_{pp} at MHz frequencies. The ultrasound actuation induces a time-harmonic pressure field $p_1 \exp(-i\omega t)$ and oscillation velocity field $v_1 \exp(-i\omega t)$, where we use the complex time-harmonic notation and where ω is the angular frequency. The viscosity of the suspension is negligible for the acoustic waves in this work, and the pressure and velocity fields in the microchannel are governed by the linear acoustic Helmholtz wave equation of inviscid fluids. By proper tuning of the applied frequency to a resonance frequency of the system, the acoustic fields become so strong that they can be used for manipulation of the particles suspended in the liquid.

The particle solutions are dilute enough that the particle-particle interactions are negligible (less than 10^{15} particles/ m^3 to avoid hydrodynamic particle-particle interaction effects¹²), and thus only single-particle physics is relevant. This comprises the acoustic radiation force acting on suspended particles, due to particle-wave scattering, and viscous drag from acoustic streaming of the carrier liquid. Both these effects are time-averaged second-order effects arising from products of the first-order fields. This work is restricted to large 5- μm -diameter particles for which the acoustic radiation force dominates and the acoustic streaming is negligible.^{7,13}

A. Microchannel single-particle acoustophoresis

Consider a single spherical particle of radius a , density ρ_p , and compressibility κ_p suspended in a liquid of density ρ_0 and compressibility κ_0 . In terms of the acoustic pressure p_1 and the oscillation velocity v_1 at the position of the particle, and given that a is much smaller than the acoustic wavelength λ , the time-averaged acoustic radiation force F^{rad} on the particle neglecting viscosity is^{14,15}

$$F^{\text{rad}} = -V \left[\frac{f_1}{2} \kappa_0 \nabla \langle p_1^2 \rangle - \frac{3f_2}{4} \rho_0 \nabla \langle v_1^2 \rangle \right], \quad (1)$$

where $f_1 = 1 - \tilde{\kappa}$ and $f_2 = (2\tilde{\rho} - 2) / (2\tilde{\rho} + 1)$ in terms of the compressibility ratio $\tilde{\kappa} = \kappa_p / \kappa_0$ and the density ratio $\tilde{\rho} = \rho_p / \rho_0$. For a transverse acoustic wave $p = p_a \cos(ky)$ of wavenumber $k = 2\pi/\lambda = \pi/w$, such that the wavelength is twice the channel width, $\lambda = 2w$, the above expression reduces to the y component¹⁶

$$F^{\text{rad}} = 4\pi^2 \Phi \frac{a^3}{w} E_{\text{ac}} \sin\left(2\frac{\pi}{w}y\right), \quad (2)$$

where E_{ac} is the time-averaged acoustic energy density and $\Phi = f_1/3 + f_2/2$ is the acoustic contrast factor.

In this work we only study such a transverse half-wave resonance, and we always have $\Phi > 0$. As a result, the radiation force is directed towards the channel center, and particles, which initially are homogeneously distributed in the microchannel as shown in Fig. 1(a), are pushed towards the vertical center plane at $y = w/2$ as shown in Fig. 1(b), where ideally they all end up.

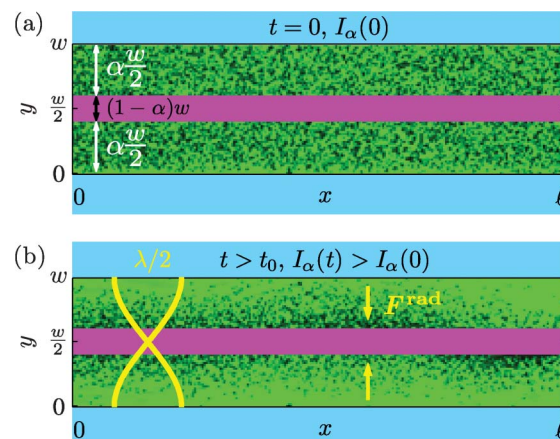


Fig. 1 Bottom-view of the straight acoustophoresis microchannel (light blue walls) of width w and length ℓ . The microchannel containing a suspension of 5- μm -diameter polyamide microbeads (black/gray dots) is illuminated from the top, resulting in a green background in the image. The particle motion is only recorded outside a band of relative width $1 - \alpha$ (magenta) along the channel center $y = w/2$, as the particle concentration outside this band remains sufficiently low throughout the entire acoustophoretic focusing process. (a) At time $t = 0$ the microbeads are homogeneously distributed throughout the channel and the light intensity of the image is $I_\alpha(0)$. (b) The microchannel is acoustically actuated in its transverse half-wave resonance (yellow) and the acoustic radiation force (yellow arrows) pushes the suspended particles to the acoustic pressure node at the vertical center plane at $y = w/2$. As the particles gradually leave the interrogation area (green) and enter the excluded band along the center plane, the light intensity of the image increases monotonically, $I_\alpha(t) > I_\alpha(0)$.

B. Transverse acoustophoretic single-particle path

Given the transverse half-wave resonance, an analytical expression for the transverse path $y(y_0, t)$ of a particle starting at y_0 at time $t = 0$ can be derived by balancing F^{rad} with the viscous Stokes drag^{7,17}

$$y(y_0, t) = \frac{w}{\pi} \arctan \left[\tan\left(\pi \frac{y_0}{w}\right) \exp\left(\frac{t}{t^*}\right) \right], \quad (3a)$$

$$t^* = \frac{3\eta}{4\Phi(\pi a/w)^2} \frac{1}{E_{\text{ac}}}, \quad (3b)$$

where η is the viscosity of the carrier liquid, and where we have introduced the characteristic time scale t^* , which is inversely proportional to the acoustic energy density E_{ac} . Here, using a channel of height $h = 110 \mu\text{m}$ and particles with diameter $2a = 4.5 \mu\text{m}$, the wall-induced drag enhancement has been neglected, because for particles at half the height in the channel the classic Faxén enhancement factor^{18,19} is $1/[1 - 1.004(2a/h)] = 1.043$, while at a quarter of the height it is $1/[1 - 0.6526(4a/h)] = 1.056$, both deviating less than 6% from unity. However, for more shallow channels the wall-induced drag enhancement may be significant.²⁰ In ref. 7 E_{ac} was determined as a fitting parameter by fitting eqn (3a) to the measured paths obtained by single-particle tracking. In Fig. 2 the transverse particle path $y(y_0, t)$ is plotted as a function of normalized time t/t^* for three different starting positions y_0 , keeping all other parameters fixed.

Inverting eqn (3a), we obtain as in ref. 7 and 21 the time t it takes a particle to move from any initial position $0 < y_0 < w/2$ to

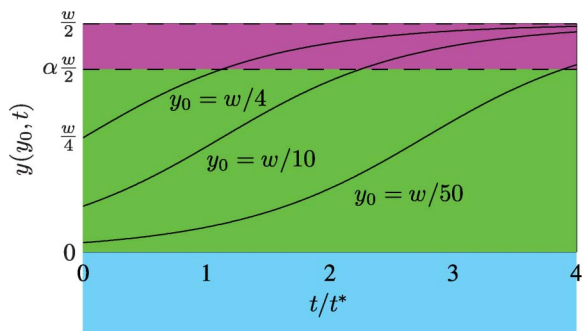


Fig. 2 Transverse particle path $y(y_0, t)$, eqn (3a), as function of normalized time t/t^* , eqn (3b). For given fixed parameters, the particle paths (black lines) are plotted for three different starting positions y_0 . The channel is divided into two regions: the interrogation area of relative width α (green), and the excluded center band of relative width $1 - \alpha$ (magenta).

any final position y at $y_0 < y < w/2$,

$$t(y_0, y) = t^* \ln \left[\frac{\tan\left(\pi \frac{y}{w}\right)}{\tan\left(\pi \frac{y_0}{w}\right)} \right]. \quad (4)$$

III. Many-particle light-intensity model

We analyze a many-particle suspension of 0.35×10^{15} particles/ m^3 (see Section VA), which is dilute enough to minimize both hydrodynamic and acoustic particle–particle interactions as well as the effect of overlapping particles located at different heights in the channel. For our system with the particle diameter $2a = 4.5 \mu\text{m}$ and channel height $h = 110 \mu\text{m}$, the threshold particle concentration C^* for particle overlapping is when exactly one particle occupies the cylindrical volume of base area πa^2 and height h , $C^* = 1/(\pi a^2 h) = 0.6 \times 10^{15} \text{m}^{-3}$, which is half of the threshold value mentioned above for particle–particle interactions. Consequently, we assume that each particle undergoes single-particle acoustophoresis as described in the previous section. To ensure that this single-particle description is valid in our analysis, we only study the particle motion in the interrogation area of relative width α (green in Fig. 1 and 2) away from the channel center, while we exclude the region of relative width $1 - \alpha$ (magenta) along the center line, where the particle concentration eventually becomes very large as all the particles end up accumulating there. In this work we found $\alpha = 0.8$ to be a good value and have used it throughout the analysis.

As illustrated in Fig. 1, all our images are bottom views of the microchannel (light blue walls). Depending on the presence of a particle, each pixel in a given image of the microchannel has a dimensionless gray-scale pixel intensity ranging from 0 (black) to 255 (white). Summing over all pixels in a given image, we obtain the total pixel intensity I_x . If no particles are present in the interrogation area of relative width α , the light intensity (green) is I_x^{max} . However, at $t = 0$ there are N_0 homogeneously distributed particles present in the interrogation area, Fig. 1 (a), and these give rise to a relative intensity reduction R ranging from zero to unity, such that the initial intensity can be written as $I_x(0) = (1 - R)I_x^{\text{max}}$. When the microchannel is ultrasonically actuated, Fig. 1

(b), the particles move towards and into the excluded center-region. Each time a particle enters the excluded region, the number $N_x(t)$ of particles left inside the interrogation area decreases by unity, and the light intensity I_x increases correspondingly. This can be expressed as

$$I_x(t) = \left[1 - R \frac{N_x(t)}{N_0} \right] I_x^{\text{max}}. \quad (5)$$

At time $t = \infty$ there are zero particles left in the interrogation area, $N_x(\infty) = 0$, and $I_x(\infty) = I_x^{\text{max}}$.

The time it takes the i th particle to move from its starting position $y_0^{(i)}$ to the excluded area at $y = \alpha w/2$ is called $\tau_x(y_0^{(i)})$, and at this time its contribution to $N_x(t)$ drops from unity to zero. Mathematically, this is expressed through the Heaviside step function $\Theta[\tau_x(y_0^{(i)}) - t]$, which by definition is unity for $t < \tau_x(y_0^{(i)})$, when the particle is visible in the interrogation area, and zero for $t > \tau_x(y_0^{(i)})$, when the particle is inside the excluded region. We can therefore write

$$N_x(t) = \sum_{i=1}^{N_0} \Theta[\tau_x(y_0^{(i)}) - t]. \quad (6)$$

If the initial number N_0 of particles is sufficiently large, typically around 10^4 as in Fig. 1 (a), it is a reasonable approximation to replace the discrete sum in eqn (6) by the ensemble average $\langle N_x(t) \rangle$ defined as the average over a homogeneous distribution of starting positions,

$$\langle N_x(t) \rangle = \frac{2N_0}{\alpha w} \int_0^{\alpha w/2} dy_0 \Theta[\tau_x(y_0) - t], \quad (7)$$

where we have used the symmetry of the system to integrate over only half the channel width. Using the dilute-limit expression (4), we find that $t < \tau_x(y_0)$ implies that the integrand in eqn (7) is unity in the interval $0 < y_0 < (w/\pi) \arctan[\tan(\pi\alpha/2)e^{-t/t^*}]$ and zero otherwise. Hence we arrive at

$$\langle N_x(t) \rangle = \frac{2N_0}{\alpha\pi} \arctan \left[\tan\left(\frac{\pi}{2}\alpha\right) e^{-t/t^*} \right]. \quad (8)$$

Taking the ensemble average of the light intensity $I_x(t)$ in eqn (5) results in the normalized light intensity,

$$\frac{\langle I_x(t) \rangle}{I_x^{\text{max}}} = 1 - R \frac{\langle N_x(t) \rangle}{N_0}, \quad (9a)$$

$$= 1 - \frac{2R}{\alpha\pi} \arctan \left[\tan\left(\frac{\pi}{2}\alpha\right) e^{-t/t^*} \right]. \quad (9b)$$

This expression is plotted in Fig. 3 as function of time t . In panel (a) the energy density E_{ac} is swept for fixed relative width α of the interrogation area, and it is clear that as the acoustic energy density increases, the suspended particles traverse faster to the channel center and the relative intensity reaches its maximum of unity faster. The opposite situation is shown in panel (b), where the relative width α is swept for fixed E_{ac} . The wider an interrogation area, the slower is the increase in intensity.

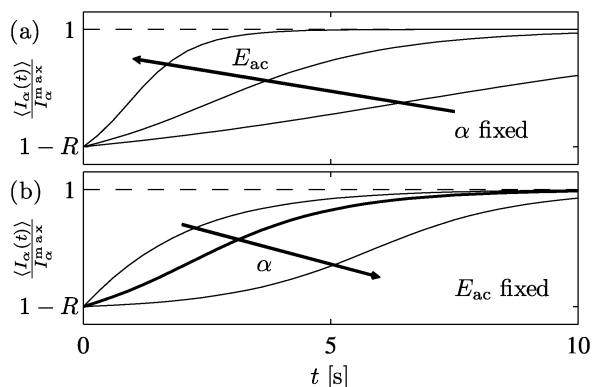


Fig. 3 Example of the normalized light intensity $\langle I_z(t) \rangle / I_z^{\max}$, eqn (9a), as function of time t and using the parameters in Table 1. (a) The energy density E_{ac} is swept (1 J/m³, 2.5 J/m³, 7 J/m³) for fixed relative interrogation-area width $\alpha = 0.8$ of the interrogation area, and it is clear that as the acoustic energy density increases, the suspended particles traverse faster to the channel center and the relative intensity reaches its maximum of unity faster. (b) The relative width α is swept (0.3, 0.8, 0.97) for fixed $E_{ac} = 2.5$ J/m³. The wider an interrogation area, the slower is the increase in intensity.

In a given experiment, the observed intensity $I_z(t)$ is identified with the theoretical ensemble average $\langle I_z \rangle$. From eqn (9b) it follows that $I_z(0) \approx \langle I_z(0) \rangle = (1 - R)I_z^{\max}$ and $I_z(\infty) \approx \langle I_z(\infty) \rangle = I_z^{\max}$. Hence, the relative intensity reduction R can be estimated from the intensity measurements as

$$R \approx 1 - \frac{I_z(0)}{I_z(\infty)}. \quad (10)$$

Once R is known, the characteristic time t^* can be found as a fitting parameter using eqn (3) to fit measured values $I_z(t)/I_z(\infty)$ versus time t . Then the acoustic energy density can be extracted from eqn (3b) if the material parameters of the microbeads are known.

Finally, the determination of t^* allows for the introduction of the exponentially re-scaled time s given by

$$s = e^{t/t^*}. \quad (11)$$

Rearranging eqn (9b) leads to the prediction that a plot of all data in the form $[1 - I_z/I_z(\infty)]/R$ versus re-scaled time s collapses on a universal curve given by

$$\frac{1}{R} \left[1 - \frac{I_z(s)}{I_z(\infty)} \right] = \frac{2}{\pi\alpha} \arctan \left[\frac{1}{s} \tan \left(\alpha \frac{\pi}{2} \right) \right]. \quad (12)$$

It follows from eqn (9a) that this particular combination of intensities can be interpreted as the relative average number of particles $n_z(s)$ left in the interrogation area,

$$\frac{1}{R} \left[1 - \frac{I_z(s)}{I_z(\infty)} \right] = \frac{\langle N_z \rangle}{N_0} = n_z(s). \quad (13)$$

IV. Intensity method for measuring the acoustic energy density

The presented intensity model can be used to measure the acoustic energy density *in situ*. The basic idea is to measure the

total pixel intensity as function of time and then fit the model described above to the data points using the acoustic energy density as a fitting parameter. The method is easily applied; all that is needed is a movie of the acoustophoretic focusing and the following algorithm:

1. Turn the CCD movie into a series of image frames.
2. Determine the total pixel intensity $I_z(t)$ of each image frame by summing the individual pixel intensities inside the interrogation area of relative width α .
3. Determine the maximum intensity $I_z^{\max} = I_z(\infty)$ from the last image in the time series.
4. Calculate the normalized intensity $I_z(t)/I_z^{\max}$.
5. Determine the initial relative intensity reduction R using eqn (10).
6. Fit expression eqn (9b) to the data $I_z(t)/I_z^{\max}$ using E_{ac} as fitting parameter by eqn (3b).

To obtain the best possible result, the measured acoustophoretic focusing should last long enough to reach a near-static bead distribution. Furthermore, α should be chosen as large as possible, but still without resulting in too many particles remaining in the interrogation area of the last image frame. Repeated measurement of the intensity curves enhances the accuracy and enables an estimate of the standard deviation of the measured energy density.

In this work the algorithm was implemented in Matlab. The Matlab script `imgs2energy.m`, we used for extracting E_{ac} via the light-intensity model, can be downloaded from the ESI.†

V. Chip, setup, and experimental procedure

A. Chip and experimental setup

Acoustophoresis microchip. We used a glass–silicon–glass chip (Gesim, Germany) as shown in Fig. 4 and described in more detail in ref. 22. The thicknesses of the top glass layer, the intermediate silicon layer, and the bottom glass layer were 0.20 mm, 0.11 mm, and 1.10 mm, respectively. In the silicon layer was etched a cavity connected to inlets and outlets by a microchannel of width $w = 328$ μm and depth $h = 110$ μm . The inlets and outlets were connected to a syringe using Teflon tubing, adapters and valves.

Acoustics driving electronics. The acoustophoresis microchip was acoustically actuated using two different in-house-built transducers, a planar transducer (PT) and an angled transducer (AT), see Fig. 4. The planar transducer was mechanically damped by a layer of epoxy, while the angled transducer was glued on a two-part wedge/quarter-cylinder aluminum mounting. The top part was connected through immersion oil to the lower part via two aluminum springs and could thus slide along the cylinder surface from 0° to 90°. This tunability feature of the coupling angle is to be used in a future work; here the angled transducer was fixed at an angle of 30°. Both the planar and angled transducer were built using PZT piezoceramic plates (Pz26, Ferroperm, Denmark) and were attached to the chip using a quick-drying and water-soluble adhesive gel (‘Tensive’, Parker Laboratories, USA). The transducers were driven by a function generator (DS345, Stanford, USA) coupled to an RF amplifier (75A250, Amplifier research, USA). The peak-to-peak voltage was monitored by an oscilloscope (TDS220, Tektronix, USA).

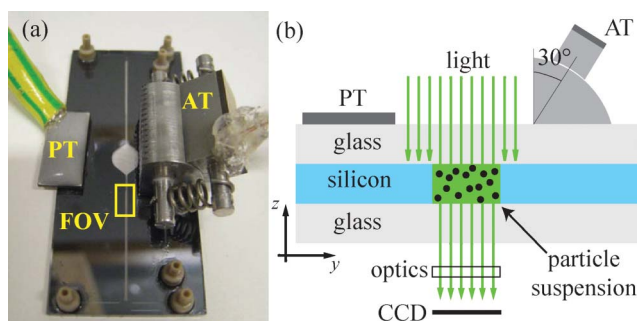


Fig. 4 (a) Photograph of the acoustophoresis glass–silicon–glass chip mounted with two ultrasonic piezo transducers, a planar transducer (PT) and an angled transducer (AT) fixed at 30°. The chip consists of a top glass layer, an intermediate silicon layer, and a bottom glass layer of thicknesses 0.20 mm, 0.11 mm, and 1.10 mm, respectively. The acoustophoretic motion in the particle suspension is observed in the yellow-square-marked field of view (FOV) of length $\ell = 1.21$ mm containing a microchannel of width $w = 328$ μm and depth $h = 110$ μm . (b) Cross-sectional sketch (not drawn to scale) of the experimental setup. The chip consists of silicon (blue) and glass (light gray) layers and is actuated by either the planar PZT transducer (PT) or the angled PZT transducer (AT) both marked by dark gray. Light (green arrows) passes through the transparent microchannel, which is recorded by a CCD camera (black) *via* an inverted microscope with a green filter cube (optics).

Temperature sensing. To observe a possible drift in resonances caused by varying temperature, the temperature was measured at the top glass layer with a T-type (copper-constant) and Teflon-insulated micro thermocouple with a total tip diameter (sensor and sheath layer) of 0.41 mm (IT-21, Physitemp Instruments, USA). Automatic monitoring of temperature data was done with the accuracy of 0.1 °C (Dostmann Electronic GmbH P655-LOG, Germany). Furthermore, the room temperature was logged throughout experimenting and both room- and chip temperatures were stable within 1 °C.

Microbead suspension. The investigated microbead suspension was a 9 : 1 mixture of Milli-Q water (with 0.01% Tween20) and a blood-mimicking fluid (EU-DFS-BMF-ver.1 for Flow Doppler Phantoms, Danish Phantom Design, Denmark) containing 5- μm -diameter polyamide microbeads (Orgasol Powders, Arkema, France). Due to its high water content, the suspension acts as pure Milli-Q water containing polyamide microbeads. The material parameters of the suspension are listed in Table 1. Using a Coulter counter, the polyamide particle concentration was measured to be $C = 3.5 \times 10^{14}$ m^{-3} with a normal distributed particle diameter of $2a = (4.5 \pm 0.7)$ μm . Despite the large size-dispersion, we used the blood-mimicking fluid because it mimicks the size-dispersion of biological cells and is inexpensive.

Imaging. The microchannel was imaged by an inverted microscope (Axiovert 40, Zeiss, Germany) with green filter cube, objective (A-Plan 10 \times /0.25 Ph1, Zeiss, Germany), and CCD camera (AxioCam HSC, Zeiss, Germany) with frame rates between 30–46 ms. To acquire a set of images from a recorded movie we used AxioVision Rel.4.8 software. The pixel resolution was 634 pixel \times 172 pixel of a channel section of size $\ell \times w =$

Table 1 Physical parameters used throughout the paper. The parameters are given for temperatures 20–25 °C

Density, water ^a	ρ_0	997 kg m^{-3}
Density, polyamide ^b	ρ_p	1030 kg m^{-3}
Speed of sound, water ^a	c_0	1497 ms^{-1}
Speed of sound, polyamide ^c	c_p	2660 ms^{-1}
Viscosity, water ^a	η	0.890 mPa s
Mean-diameter, polyamide microbeads ^d	$2a$	(4.5 ± 0.7) μm
Microbead concentration in suspension ^d	C	3.5×10^{14} m^{-3}
Compressibility, water ^e	κ_0	448 TPa^{-1}
Compressibility, polyamide ^e	κ_p	137 TPa^{-1}
Compressibility factor, water/polyamide	f_1	0.69
Density factor, water/polyamide	f_2	0.02
Contrast factor, $\Phi = f_1/3 + f_2/2$	Φ	0.24

^a Water at 25 °C: CRC Handbook of Chemistry and Physics
^b ORGASOL® 5 μm : <http://r427a.com/technical-polymers/orgasol-powders/technical-data-sheets>
^c Nylon 6-6: CRC Handbook of Chemistry and Physics.
^d Measured by Coulter Counter.
^e Calculated from density and speed of sound as $\kappa = 1/(\rho c^2)$.

1209 $\mu\text{m} \times 328$ μm . Therefore 1 pixel corresponds to 1.9 μm implying that a 4.5 μm diameter particle will roughly cover 10 pixels. This is roughly the same as the optical resolution of 1.3 μm of the objective used. Given the above microbead concentration C and a relative interrogation-area width $\alpha = 0.8$, we can estimate the number N_0 of visible microbeads to be $N_0 = \alpha C \ell w h \approx 1.2 \times 10^4$.

Isolated-particle prediction of the total light-intensity reduction.

To verify that optical many-particle effects, such as light scattering and particle shadowing, can be neglected, we predict the total relative intensity reduction R based on the particle concentration C and the intensity reduction of isolated particles. In Fig. 5 (a) we show a single image frame where the microbeads have traversed acoustophoretically half way towards the center of the microchannel. The image clearly shows how single particles are less distinguishable as they move closer together near the center plane of the channel. In the image we mark a region (black square) where we investigate 5 pixel \times 5 pixel square regions surrounding each of 41 isolated particles. Fig. 5 (b) shows 14 such squares. On average a 5 pixel \times 5 pixel square containing a single particle has a total dimensionless, gray-scale pixel intensity of $I_p = (3.3 \pm 0.2) \times 10^3$. When all the particles

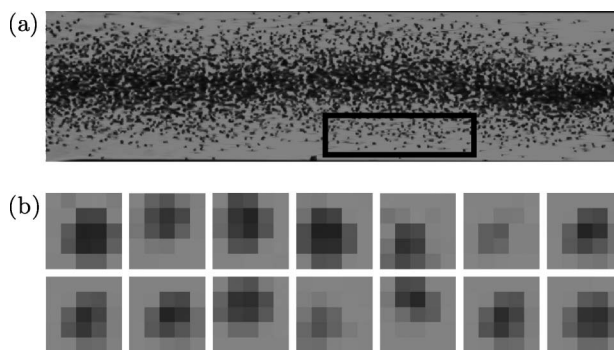


Fig. 5 (a) Gray-scaled experimental image where the microbeads have traversed acoustophoretically half the way towards the center of the microchannel. Inside the black rectangle all isolated particles are identified and their pixel intensities are analyzed within a 5 pixel \times 5 pixel square. (b) 5 pixel \times 5 pixel square views of 14 of the 41 isolated microbeads in the black rectangle marked in panel (a).

by acoustophoresis have traversed into the excluded center region, we obtain the maximum total pixel intensity $I_z^{\max} \approx 1.3 \times 10^7$ corresponding to an intensity per pixel of 149 and implying $I_{\text{ref}} = 3.7 \times 10^3$ for an empty 5 pixel \times 5 pixel square. Finally, we predict the relative intensity reduction $R = N_0 (I_{\text{ref}} - I_p)/I_z^{\max} \approx 0.42 \pm 0.16$. Notice, this is an upper estimate for R as it excludes effects such as particle shadowing, which will decrease R .

B. Experimental procedure

Stop-flow particle-focusing experiments. The polyamide microbead suspension was injected into the chip manually using a glass syringe. The flow was stopped and a field of view section (yellow rectangle FOV in Fig. 4 (a)) in the straight part of the acoustophoresis microchannel was observed. While actuating one of the two transducers close to the transverse half-wave resonance of the microchannel, the acoustophoretic particle motion was recorded with the CCD camera. A movie typically lasted 30 s comprising about 600 image frames. The actuation frequency was modulated linearly²³ with a rate of 1 kHz from 2.06 MHz to 2.16 MHz around the center frequency 2.11 MHz.

Energy density determination. We use the intensity method described in Section IV to extract the acoustic energy density from a given acoustophoretic focus experiment. As the variation Δa in particle radius a is large (about 15%), we extract E_{ac} for the particle radii a , $a + \Delta a$, and $a - \Delta a$, with $\Delta a = 0.7 \mu\text{m}$.

Scan in PZT voltage. Our experimental study consists of five independent experiment series, where we scanned the PZT voltage U_{pp} of one of the two transducers in the range from 0 to 23 V. For each driving voltage, we performed the above described stop-flow focus experiment. In the two first experiment series, we drove the angled transducer AT, while in the last three series, we drove the planar transducer PT. Each experiment series consisted of typically 16 particle-focusing experiments (16 driving voltages) resulting in a total of 88 acoustophoretic focusing experiments for the experimental study.

VI. Results

A. Validation of the light-intensity method

To validate the light-intensity method described in Section IV, we measure the acoustic energy density using the particle tracking method.⁷ In the first experimental series for the planar transducer at $U_{\text{pp}} = 18.9 \text{ V}$, we use the freeware particle tracking program Tracker 4.61 to track 20 microbeads and using the tracking method, we obtain an acoustic energy density $E_{\text{ac}} = (1.45 \pm 0.5) \text{ J m}^{-3}$. Using the light-intensity method, we obtain the acoustic energy density $E_{\text{ac}} = (1.4 \pm 0.4) \text{ J m}^{-3}$. In conclusion, the obtained acoustic energy density agrees well with that of the previously reported tracking method. For both methods, the presented uncertainty is due to the size dispersion of the particles.

The light-intensity method turned out to be a simple, rapid, and robust method compatible with low- or mid-ranged microscopes yielding moderate resolution images of high particle concentrations. In contrast, the tracking method was tedious and micro-PIV was impossible.

B. Scanning the PZT voltage

We use the intensity method described in Section IV to extract the acoustic energy density from each of the 88 particle-focusing experiments in our experimental study in Section IV. In Fig. 6 (a) we plot the normalized light-intensity curves $I_x(t)/I_x(\infty)$ for every third (for clarity) of the 88 acoustophoretic focusing experiments of either driving the angled transducer (red points) or driving the planar transducer (blue points). At starting time $t = 0$, it is seen from eqn (10) that the mean of the relative intensity reduction $R = 0.36 \pm 0.07$. This value of the relative intensity reduction is close to, but deviates as expected slightly from, the upper prediction $R = 0.42 \pm 0.16$ in Section V A.

In Fig. 6 (b) we show the measured acoustic energy densities E_{ac} (red and blue disks) as function of the driving voltage squared U_{pp}^2 . The energy density is extracted using the mean particle diameter $2a = 4.5 \mu\text{m}$ and is shown for each of the five U_{pp} -scanning experimental series. Within each experiment series, we observe that the energies scale with U_{pp}^2 as expected⁷, and to the data we fit a straight line $E_{\text{ac}} = \beta U_{\text{pp}}^2$ (black line). Similarly, we plot dashed lines when the energy densities are extracted using particle radius of $a + \Delta a$ and $a - \Delta a$, respectively, with $\Delta a = 0.7 \mu\text{m}$.

Using the fitted energy densities, we find the re-scaled time s given by eqn (11) and subsequently plot the intensity data in the form $[1 - I_x/I_x(\infty)]/R$ versus s . The data points collapse on the universal curve for the relative average number $n_x(s)$ of particles given by eqn (13) thereby providing a consistency check of the underlying single-particle assumption.

VII. Discussion

The simple and rapid light-intensity method to determine the acoustic energy density in acoustofluidic microsystems is based on a large number of particles, which leads to a reduction of statistical errors. The method is especially useful when analyzing moderate-resolution images of high particle concentration, where tracking- and micro-PIV methods are difficult to apply.

As we have used microbeads with a wide size distribution (about 15%), our estimates of the acoustic energy densities have similar high relative uncertainties. This is indicated by the dashed lines in Fig. 6 (b). However, we see from the scatter of the data points around the expected βU_{pp}^2 -curve that, for a fixed value of the particle radius, the statistical uncertainty, beyond that due to particle dispersion, is about 4%. This indicates the potential for high precision measurements using the method on monodisperse particle suspensions.

The method is subject to some uncertainties: (i) The particle concentration has to be low enough to maintain single-particle acoustophoresis by avoiding clustering as well as acoustic and hydrodynamic particle-particle interactions (below 10^{15} particles/m³). It must also be low enough to neglect optical many-particle effects (below 0.6×10^{15} particles/m³ to avoid shadowing). We checked explicitly in this work that the total intensity reduction obtained from an isolated-particle analysis coincides well with that obtained from the full many-particle images at our density of 0.35 ± 10^{15} particles/m³. (ii) The acoustic wave has to be a 1D planar transverse standing wave to allow for the use of the analytical expressions in the light-intensity model. In some works, such a wave is not intended, for

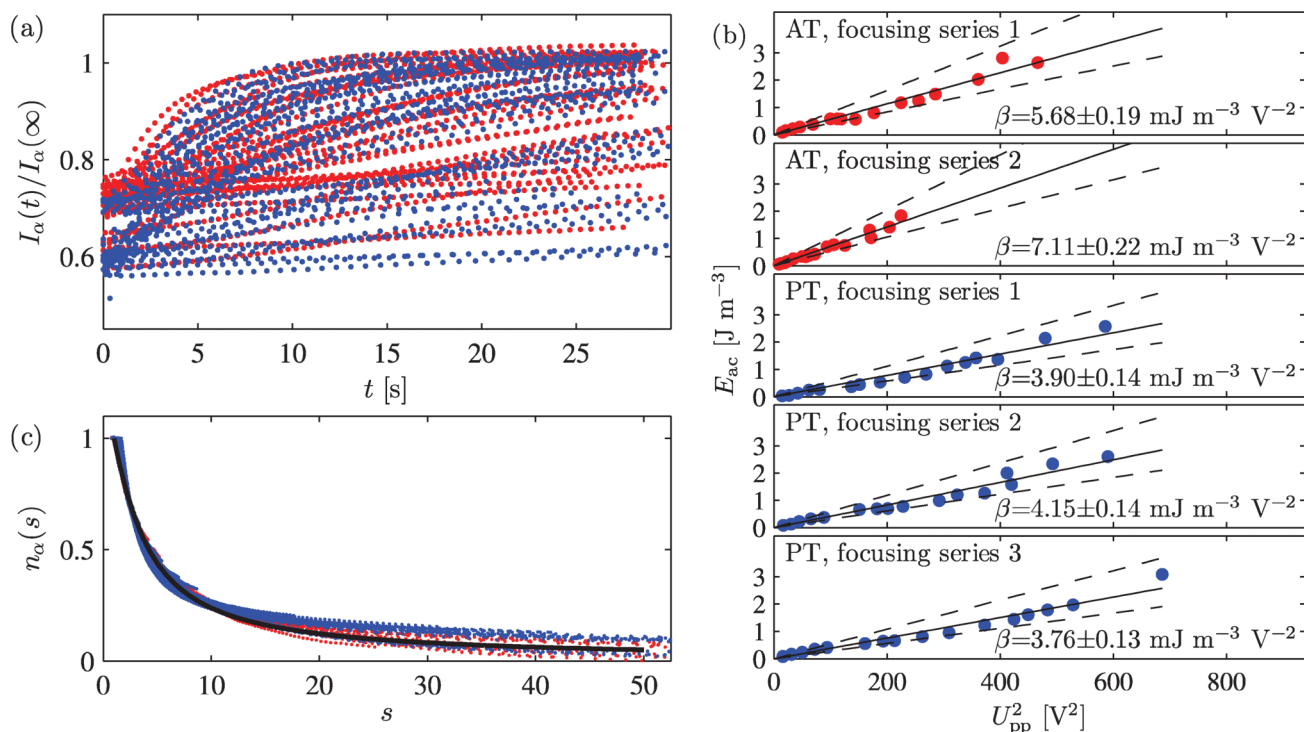


Fig. 6 Analysis of the five independent experimental series comprising of 88 individual acoustophoretic focusing experiments, where the piezo voltage U_{pp} is scanned from 0 to 23 V. (a) Normalized total intensity curves $I_\alpha(t)/I_\alpha(\infty)$ for every third (for clarity) of the 88 experiments of either driving the angled transducer (red points) or driving the planar transducer (blue points). (b) Fitted acoustic energy densities E_{ac} (red and blue disks) as function of the driving voltage squared U_{pp}^2 for each of the five experimental U_{pp} -scanning series. Within each of the voltage sweep series, a voltage square law $E_{ac} = \beta U_{pp}^2$ (black lines) is fitted to the data points. Also shown are two similar fits using the bead radius $a + \Delta a$ (lower dashed line) and $a - \Delta a$ (upper dashed line) with $\Delta a = 0.7 \mu\text{m}$. (c) The data points in panel (a) plotted *versus* the re-scaled time s , given by eqn (11) and E_{ac} from panel (b), collapse onto the universal curve $n_\alpha(s)$ for the relative average number of particles given in eqn (13).

example to achieve particle agglomeration in a point,^{22,24} and for those, after excluding the appropriate nodal line regions of more complex shape, the method can only be used to obtain relative figures of merit without the benefit of analytical predictions. In other works, where a 1D planar transverse standing wave is intended, such a wave may still be difficult to achieve, as shown in recent work by Augustsson *et al.*¹¹ In the present work we overcame this challenge by using frequency-modulation to average over a large number of resonances all with the transverse wave feature, but with different modal patterns along the axial length of the channel. The choice of excluding the center part in the images containing the focused particles further contributes to minimize the effects of particle–particle interactions or weak axial components in the acoustic field perpendicular to the transverse standing wave used in the model. (iii) The focus experiment has to be carried out with acoustophoretic particle velocities large enough to avoid sedimentation and thus avoid influence on the particle motion by the presence of the bottom channel wall. In our work, the wall-induced drag enhancement was less than 6% for the center half of the channel volume, thus the systematic under-estimation of the acoustic energy density is of the same order. If a more accurate estimate of the energy is required, a height-dependent Faxén correction must be included in the calculation of the single-particle tracks.²⁰ (iv) The temperature has to be stable enough to avoid drift in acoustic resonances.¹¹

In this work the method was applied to a trans-illuminated microchannel. However, in principle, the method can be applied to setups utilizing reflected light in, say, chips where only the lid is transparent.

VIII Conclusions

This paper describes a simple and rapid method for *in situ* determination of the acoustic energy density by observing the increase in light intensity as suspended particles undergo acoustophoresis. The method relies on a theoretical model of averaging over many particles each being subject to single-particle acoustic motion, and it has been validated with the single-particle tracking method. We have shown by proper re-scaling that the re-scaled light intensity *versus* re-scaled time fall on a universal curve predicted by ensemble averaging over acoustophoretic single-particle paths. Compared to other methods, the light-intensity method is especially well suited for images of many particles and of moderate image resolution. We envision it as a main tool in future characterization and optimization of microchips and transducers used for acoustophoresis. Moreover, it has the potential for use in biological applications, such as measurements of the acoustic contrast factor of an ensemble of cells. This would enable a simple and fast method for measuring the stiffness of *e.g.* blood cells, which is a parameter of clinical significance in a wide range of medical conditions.²⁵

Note added after first publication

This article replaces the version published on 20th April 2012, which contained errors in eqn (4).

Acknowledgements

This research was supported by the Danish Council for Independent Research, Technology and Production Sciences, Grant No. 274-09-0342, the Swedish research council, Grant No. 2011-5230, and the EU-FP7 project "RAPP-ID" in the Innovative Medicines Initiative (IMI).

References

- 1 J. Friend and L. Y. Yeo, *Rev. Mod. Phys.*, 2011, **83**, 647.
- 2 H. Bruus, J. Dual, J. Hawkes, M. Hill, T. Laurell, J. Nilsson, S. Radel, S. Sadhal and M. Wiklund, *Lab Chip*, 2011, **11**, 3579.
- 3 M. Wiklund, P. Spégel, S. Nilsson and H. M. Hertz, *Ultrasonics*, 2003, **41**, 329.
- 4 S. P. Martin, R. J. Townsend, L. A. Kuznetsova, K. A. J. Borthwick, M. Hill, M. B. McDonnell and W. T. Coakley, *Biosens. Bioelectron.*, 2005, **21**, 758.
- 5 J. Hultström, O. Manneberg, K. Dopf, H. M. Hertz, H. Brismar and M. Wiklund, *Ultrasound Med. Biol.*, 2007, **33**, 145.
- 6 M. Wiklund, C. Günther, R. Lemor, M. Jäger, G. Fuhr and H. M. Hertz, *Lab Chip*, 2006, **6**, 1537.
- 7 R. Barnkob, P. Augustsson, T. Laurell and H. Bruus, *Lab Chip*, 2010, **10**, 563.
- 8 P. Augustsson, R. Barnkob, C. Grenvall, T. Deierborg, P. Brundin, H. Bruus and T. Laurell, in Proc. 14th MicroTAS, 3–7 October 2010, Groningen, The Netherlands, edited by S. Verporte, H. Andersson, J. Emneus, and N. Pamme (CBMS, 2010) pp. 1337–39.
- 9 R. Barnkob, P. Augustsson, C. Magnusson, H. Lilja, T. Laurell and H. Bruus, in Proc. 15th MicroTAS, 2–6 October 2011, Seattle (WA), USA, edited by J. Landers, A. Herr, D. Juncker, N. Pamme, and J. Bienvenue (CBMS, 2011) pp. 127–129.
- 10 D. Hartono, Y. Liu, P. L. Tan, X. Y. S. Then, L.-Y. L. Yung and K.-M. Lim, *Lab Chip*, 2011, **11**, 4072.
- 11 P. Augustsson, R. Barnkob, S. T. Wereley, H. Bruus and T. Laurell, *Lab Chip*, 2011, **11**, 4152.
- 12 C. Mikkelsen and H. Bruus, *Lab Chip*, 2005, **5**, 1293.
- 13 S. M. Hagsäter, T. G. Jensen, H. Bruus and J. P. Kutter, *Lab Chip*, 2007, **7**, 1336.
- 14 L. P. Gorkov, *Soviet Physics-Doklady*, 1962, **6**, 773.
- 15 M. Settnes and H. Bruus, *Phys. Rev. E*, 2012, **85**, 016327.
- 16 K. Yosioka and Y. Kawasima, *Acustica*, 1955, **5**, 167.
- 17 M. Kumar, D. Feke and J. Belovich, *Biotechnol. Bioeng.*, 2005, **89**, 129.
- 18 H. Faxén, *Ann. Phys.*, 1922, **68**, 89.
- 19 J. Happel and H. Brenner, *Low Reynolds number hydrodynamics with special applications to particulate media* (Martinus Nijhoff Publishers, The Hague) 1983.
- 20 M. Koklu, A. C. Sabuncu and A. Beskok, *J. Colloid Interface Sci.*, 2010, **351**, 407.
- 21 M. S. Limaye and W. T. Coakley, *J. Appl. Microbiol.*, 1998, **84**, 1035.
- 22 J. Svennebring, O. Manneberg, P. Skafte-Pedersen, H. Bruus and M. Wiklund, *Biotechnol. Bioeng.*, 2009, **103**, 323.
- 23 O. Manneberg, B. Vanherberghen, B. Onfelt and M. Wiklund, *Lab Chip*, 2009, **9**, 833.
- 24 D. Bazou, L. A. Kuznetsova and W. T. Coakley, *Ultrasound Med. Biol.*, 2005, **31**, 423.
- 25 F. C. Mokken, M. Kedaria, C. P. Henny, M. R. Hardeman and A. W. Gelb, *Ann. Hematol.*, 1992, **64**, 113.